Pergamon

0301-9322(95)00015-1

Int. J. Multiphase Flow Vol. 21, No. 5, pp. 733–753, 1995

0301-9322/95 $9.50 + 0.00

LINEAR STABILITY OF STRATIFIED CHANNEL FLOW

W. C. KURU, M. SANGALLI, D. D. UPHOLD and M. J. McCREADY
Department of Chemical Engineering, University of Notre Dame, Notre Dame, IN 46556, U.S.A.

(Received 20 April 1994; in revised form 16 February 1995)

Abstract—Linear stability of horizontal gas–liquid stratified flow was solved using a tau spectral method that is valid for all wavenumbers. Pressures of 0.1–10 atm and liquid viscosities of 1–600 cP were examined. Comparison of these results with Kelvin–Helmholtz, integral momentum and rigorous long wave expansion approaches indicates that the approximate models do not correctly predict the point of neutral stability. The discrepancies in the models are due to more than differences in the calculation of interfacial perturbation stress components and differences in the base states. Stability predictions that include gas phase turbulence, as modeled with either a polynomial velocity profile or with imposed boundary conditions obtained from measured pressure and shear stress variations, are similar to laminar results if the interfacial stress and liquid depth are the same. The long wave stability boundary is found to correlate well for different channel height, density ratio and viscosity ratio, using a gas superficial Froude number corrected with a square root of density ratio and a liquid superficial Froude number. For gas–liquid channel flow waves that grow fastest typically have dimensionless wavenumbers of order unity. Their growth rate scales as a corrected gas Reynolds number to the first power. If the gas–liquid depth ratio is less than approximately one, long waves can be unstable before moderate wavelength waves. Under conditions where unstable moderate wavelength waves appear within a couple of meters, it can take 20–50 times this length for slowly growing long wavelength waves, which can destroy regime stability, to appear.

Key Words: stratified flow, linear stability, flow regime transition

1. INTRODUCTION

To design and operate pipelines or process equipment, knowledge of the flow regime is essential because important flow characteristics such as average and fluctuating pressure drop, steadiness of throughput and uniformity of wall cooling or heating vary greatly depending upon the regime. Unfortunately, prediction of flow regime is a difficult problem that has not yet been solved. Current procedures include use of regime maps (e.g. Mandhane *et al.* 1974) or general calculation procedures based on transitions from stratified flow (e.g. Taitel & Dukler 1976). Maron & Brauner (1990), Barnea (1991) and Crowley *et al.* (1992, 1993) use versions of averaged momentum equations to predict transitions from stratified to slug and annular flow. The flow maps are limited because they are plots of dimensional variables and it can be seen from Lin & Hanratty (1986), if the pipe diameter is changed, the boundaries move—as would be expected—on dimensional grounds. Three issues are important about stability procedures. First, because all the methods employ approximate equations (e.g. inviscid, modified inviscid or one-dimensional average equations) it is not clear that the equations are predicting the stability of a real disturbance. The second issue concerns the consistency of the models. For example, Barnea's (1991) equations are one-dimensional so that the inherent assumption is that wavelength is long compared to the phase depths. However, these equations predict that the fastest growing wavenumber may be of order one—which seems inconsistent. A third question is whether the observed transitions are caused by linear instabilities.

Use of approximate equations for calculating stability has been justified because even the linearized Navier–Stokes disturbance equations for laminar flow are difficult to solve. Turbulence adds to this complexity as does the perception that it is necessary to calculate the linear stability of a secondary (e.g. long wavelength) disturbance when the interface is covered by moderate wavelength waves, to predict regime transitions. In recent years, improved numerical and analytical techniques make it possible to obtain solutions to the complete differential problem in the form of the Orr–Sommerfeld equation. Consequently, it would be interesting to examine the predictions of the exact equations and compare them to the predictions of approximate models.

Kordyban & Ranov (1970) and Taitel & Dukler (1976) used modifications of Kelvin–Helmholtz instability to predict slug formation. The most unstable wavelength for Kelvin–Helmholtz instability is about 1.7 cm for air–water and is thus not a long wavelength wave. Lin & Hanratty (1986) assumed that slugs form from continued growth of long wavelength waves and used a linear stability theory that employs integral momentum balances to predict the onset of slugging. More recent papers by Andritsos *et al.* (1989) and Fan *et al.* (1993) suggest that the picture is more complicated. They observe conditions where moderate waves appear to grow rapidly into slugs and other conditions where the wavelength has doubled at least once and grown with distance before a slug is formed. As a consequence, accurate prediction of linear behavior for all wavenumbers is needed.

Linear stability analyses based on the Orr–Sommerfeld equation have been done for the case of unconfined flows by Valenzuela (1976), Kawai (1979) and Gastel *et al.* (1985). Gastel *et al.* (1985) shows that while the assumed shapes of the turbulent liquid and gas velocity profiles affect the results, linear predictions of growth rates match the experiments rather well. Linear analyses relevant to two-layer channel flows include Cohen & Hanratty (1965), Craik (1966), Yih (1967), Hooper & Boyd (1983), Hinch (1984), Hooper (1984), Renardy (1985), Yiantsios & Higgins (1987) and Su & Khomami (1992). Hanratty & McCready (1995) report that the spatial growth rates of Sangalli *et al.* (1992) match linear predictions within the accuracy of the data. Jurman *et al.* (1992) find that measured wave speeds match the linear predictions. These studies provide important physical insights and confirm its validity at describing quantitative aspects of the linear growth/decay process.

In this paper, we examine the linear stability of stratified channel flow using the Orr–Sommerfeld equation and complete two-phase boundary conditions. Calculations are done at conditions and fluid properties typical of horizontal gas–liquid flow. We examine the long wave limit, where the problem can be solved analytically using a perturbation approach, and the entire wavenumber range using a numerical spectral approach. Our primary goals are to obtain some general results that can be used without doing complete calculations and to gain insight into important physical effects. It is found that moderate wavelength waves are unstable first for most conditions; a correlative procedure for determining the growth rate of the fastest growing waves is introduced. The long wave stability boundary for different conditions is found to correlate reasonably well using density corrected gas and liquid Froude numbers. The influence of pressure on the growth rates and stability boundaries is discussed. The effect of turbulence in the gas phase is investigated using a polynomial profile for the gas (Pai 1953) and through the use boundary conditions on the liquid that are obtained from stress correlations for turbulent flow over solid waves. It is found that the primary effect of turbulence is through alterations in the base state; for turbulent flow, the pressure drop and interfacial shear are higher than laminar flow for fixed gas Reynolds number. Furthermore, both the one-dimensional momentum model and the Kelvin–Helmholtz models differ substantially from the predictions of the full Navier–Stokes equations.

2. THEORY

Waves in channel flow exhibit spatial growth. However, as discussed by Hanratty & McCready (1995), it is usually sufficient to consider temporal growth and convert this to spatial growth with the group velocity if necessary. Far from neutral stability there may be some quantitative error, but the qualitative behavior will be similar.

2.1. Full equations

The flow situation of interest is shown in figure 1. The calculations will be given for a two-dimensional flow although a Squire transformation (Blennerhassett 1980) is possible to account for the behavior of three-dimensional disturbances. The equations and boundary conditions for a two-layer laminar stratified flow in a channel have been given by Yih (1967), Blennerhassett (1980), Yiantsios & Higgins (1988) among others. In terms of the disturbance stream function (using Blennerhassett's notation) these become,

$$\Phi = \Phi' = 0 @ y = 1, \qquad [1a]$$

$$\phi = \Phi, \quad @y = 0, \tag{1b}$$

$$\phi' - \frac{u_b'\phi}{(u_b(0) - c)} = \Phi' - \frac{U_b'\Phi}{(u_b(0) - c)}, \quad @y = 0, \tag{1c}$$

$$\phi'' + k^2\phi = \mu(\Phi'' + k^2\Phi), \quad @y = 0. \tag{1d}$$

$$\frac{1}{\nu R}(\phi''' - 3k^2\phi') + ik(\phi u_b' - \phi'(u_b(0) - c)) + \frac{ik\phi}{(u_b(0) - c)}\frac{(F + k^2T)}{R^2} =$$

$$\frac{\rho}{R}(\Phi''' - 3k^2\Phi') + \rho ik(\Phi U_b' - \Phi'\sigma) + \frac{i\rho k\phi}{(u_b(0) - c)}\frac{F}{R^2}, \quad @y = 0, \tag{1e}$$

$$ik(u_b - c)(\Phi'' - k^2\Phi) - ikU_b''\Phi = R^{-1}(\Phi^{iv} - 2k^2\Phi'' + k^4\Phi), \text{ for } 0 \leqslant y \leqslant 1 \tag{1f}$$

$$ik(u_b - c)(\phi'' - k^2\phi) - iku_b''\phi = (\nu R)^{-1}(\phi^{iv} - 2k^2\phi'' + k^4\phi), \text{ for } -1/d \leqslant y \leqslant 0 \tag{1g}$$

$$\phi = \phi' = 0, \quad @y = -d^{-1}. \tag{1h}$$

The viscosity ratio is $\mu = \mu_2/\mu_1$, the density ratio is $\rho = \rho_2/\rho_1$, the ratio of kinematic viscosities is ν, $\sigma = u_b(0) - c$ and the depth ratio is $d = D_2^\dagger/D_1^\dagger$. The average dimensionless velocity profiles are u_b for the liquid and U_b for the gas; the wavenumber is k which is made dimensionless with $D_2^\dagger$. In these equations, ϕ and Φ are the disturbance stream functions defined from,

$$U = \Phi'(y)\exp[ik(x - ct)], \; u = \phi'(y)\exp[ik(x - ct)],$$

$$V = -ik\Phi(y)\exp[ik(x - ct)], \; v = -ik\phi(y)\exp[ik(x - ct)], \tag{2}$$

where lower case variables refer to the lower phase and upper case variables refer to the upper phase. The term U is the x direction disturbance velocity of the gas, which is the primary flow direction and V is the y direction velocity. The height is made dimensionless with the upper phase height, and the origin is located at the interface. The characteristic velocity is a mean velocity defined as

$$U_m^\dagger = \frac{1}{D_1^\dagger + D_2^\dagger}\left(\int_{-D_1^\dagger}^{0} u_b^\dagger \, dy^\dagger + \int_0^{D_2^\dagger} U_b^\dagger \, dy^\dagger\right) \tag{3}$$

where $y^\dagger$ is the dimensional y direction, $u_b^\dagger$ is the dimensional liquid velocity profile and $U_b^\dagger$ is the dimensional gas velocity profile. The parameters R, F and T are defined as

$$R = \frac{U_m^\dagger D_2^\dagger}{\nu_2}, \tag{4}$$

$$F = \frac{gD_2^{\dagger 3}}{\nu_2^2}, \tag{5}$$

$$T = \frac{SD_2^\dagger}{\rho_1 \nu_2^2}. \tag{6}$$

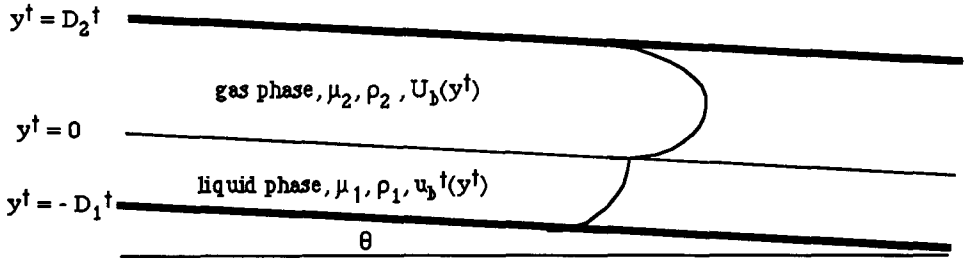

Figure 1. Diagram of flow configuration for concurrent gas–liquid flow.

The Reynolds number, R, is defined similarly to other studies but F and T are essentially Froude and Weber numbers multiplied by R^2. The wave speed is c, g is the gravity constant and S is the surface tension coefficient.

No analytical solution to the eigenvalue problem given by these equations has been found, and because the maximum growth rate occurs at $k = O(1)$ it is usually not possible to employ an expansion in either k, $1/k$ or $1/k\mathrm{R}$ to obtain an analytical solution that is useful for determining the maximum growth rate. Consequently, we have solved the eigenvalue problem using a Chebyshev tau spectral technique similar to Su & Khomami (1992) that was implemented in Matlab®. To eliminate the infinite eigenvalues that occur because the eigenvalue does not appear in all the equations, we made use of an algebraic reduction after employing the spectral expansion. To remove the spurious modes (Orszag 1971) that arise because of discretization of the third and fourth order derivatives, we adapted to our problem the more sophisticated modified tau method proposed by Gardner *et al.* (1989), which consists of a factorization of the differential operator, and successive elimination of the additional unknowns that are introduced. The method represents an alternative discretization of the differential operator resulting in a different algebraic eigenvalue problem that is resistant to the appearance of spurious modes. The code then converged for all conditions and provided the speed and growth rate for all eigenvalues.

2.2. *Long wave expansion*

Stability of long wavelength waves has been used as a criterion for slug formation by Lin & Hanratty (1986). This idea is very plausible because even though non-linear effects can transfer energy from moderate wavelength to long waves (Jurman *et al.* 1992) it is unlikely that a wave that is long enough to grow into a slug, could reach a large amplitude unless a linear process is also involved. Blennerhassett (1980) solves the long wavelength stability problem up to order k^1 analytically using an adjoint operator method. The long wavelength results presented below are obtained from his paper for laminar flow and by modifying the average profile when a polynomial profile is used. Note that for flows of interest, a theory accurate to $O(k^1)$ corresponds to a wave that could be 10 m or longer which may not have any relevance for an actual flow. However, if long wave theory predicts instability, it is likely that all waves up to the moderate wavelength region are unstable. Figure 11 shows that this is not always true. If long wave theory predicts stability, generally the growth rate gets more negative as k increases because the wave speed is increasing. The speed increase occurs until the liquid depth–wavelength ratio becomes of $O(0.1)$. Once the speed stops its rapid increase with wavenumber, the growth rate usually increases and wave modes can become unstable. Considering these arguments, long wave theory ordinarily gives useful information about realistic waves.

2.3. *Macroscopic momentum equation*

Lin & Hanratty (1986) give the integral momentum balance equations (or one-dimensional equations) for a two-layer channel flow and show how to obtain the neutral conditions. Crowley *et al.* (1992) give similar equations and procedures for calculations of regime transitions from stratified to annular flow and slugging. Equations of this type are obtained by averaging over the y direction and as a result will not exactly represent the flow fields. They are intended to predict disturbances that are long compared to the channel or height. However, it is not clear how close to the full differential equations these predictions will be, nor is the best procedure for comparing the two approaches obvious. To make this assessment, they are compared below using both dimensional plots and a dimensionless plot.

2.4. *Kelvin–Helmholtz model*

Kelvin–Helmholtz (Drazin & Reid 1981) stability model assumes that the flow is inviscid and therefore LaPlace equations for the potential function govern the flow field. Because the velocity profiles are flat, there is a discontinuity in velocity at the interface. Instability is predicted when the Bernoulli effect is large enough to overcome the restoring forces of gravity and surface

tension. The dispersion relation for this model when the effect of finite channel size is included is

$$c = \frac{\rho_1 \bar{u}_1^\dagger \coth[k^\dagger D_1^\dagger] + \rho_2 \bar{U}_2^\dagger \coth[k^\dagger D_2^\dagger]}{\rho_1 \coth[k^\dagger D_1^\dagger] + \rho_2 \coth[k^\dagger D_2^\dagger]}$$

$$\pm \frac{i}{k^\dagger(\rho_1 \coth[D_1^\dagger k] + \rho_2 \coth[D_2^\dagger k])} * [-k^{\dagger 2}\rho_1\rho_2 \coth[k^\dagger D_1^\dagger]\coth[k^\dagger D_2^\dagger](\bar{u}_1^\dagger - \bar{U}_2^\dagger)^2$$

$$+ k^\dagger \boldsymbol{g}(\rho_1 - \rho_2)(\rho_1 \coth[k^\dagger D_1^\dagger] + \rho_2 \coth[k^\dagger D_2^\dagger])$$

$$+ Sk^{\dagger 3}(\rho_1 \coth[k^\dagger D_1^\dagger] + \rho_2 \coth[k^\dagger D_2^\dagger])]^{1/2}. \quad [7]$$

In this equation $\bar{U}_2^\dagger$ is the average dimensional gas velocity, $\bar{u}_1^\dagger$ is the average liquid velocity and $k^\dagger$ is the dimensional wavenumber. This agrees with Barnea's (1991) inviscid analysis only if the wavenumber goes to 0. The Kelvin–Helmholtz model predicts that for air–water flows at conditions close to neutral stability, the most unstable wavelength is 1.7 cm—which is neither short nor long for typical size conduits.

2.5. Methods for dealing with turbulent flow

Most process flows have at least one phase that is turbulent. In this section we consider two ways for approximating the effect that gas phase turbulence will have on linear stability behavior. The first is the "divided attack" suggested by Benjamin (1957) and implemented for a stability problem by Cohen & Hanratty (1965) and Craik (1966). It involves solving the Orr–Sommerfeld equation in the liquid phase and includes the effect of gas flow through the pressure and shear stress boundary conditions. The gas phase is solved separately as flow over a solid wavy surface. Hanratty (1983) suggests that correlations of measurements of pressure and shear variations for turbulent flow over solid wavy surfaces can be used. Using boundary conditions from stress correlations for a solid surface has been justified by the small density, 1/890, and viscosity, 1/56, ratios for air–water. The magnitude of the error in doing this has not been established and it cannot be obtained from analytical expressions for the eigenvalue problem (e.g. [1]) because the limit as $\mu \to 0$ is not equivalent to the divided attack.

This method is implemented here by solving the Orr–Sommerfeld equation in the liquid phase with a tau–spectral method and using the stress correlations for model D^* given by Abrams (1984) to predict the pressure and shear stress boundary conditions. The D^* model provides a good fit to measured magnitudes and phase angles of the shear stress and pressure fluctuations for turbulent flow over solid waves. Because no governing equation for the gas phase is used, it is necessary to specify friction velocity, v^*, liquid Reynolds number $R_L = D_1^\dagger \bar{u}_1^\dagger / \nu_1$, and $D_1^\dagger$, the liquid depth, as input parameters (even though in the two-layer problem only two of them are independent).

To examine the inherent accuracy of the divided attack or imposed stress approach, it is possible to solve for laminar flow over a solid wavy wall, and then use the calculated stresses in the equations for the liquid phase. This problem can be solved for the long wave limit using a perturbation method; it gives an unambiguous comparison of the exact two-phase solution with the divided attack for linear stability. We have also implemented the divided attack in our numerical code so that the use of turbulent stresses can be compared to laminar stresses for all wavenumbers.

The boundary conditions are formulated as shown by Cohen & Hanratty (1965) or Craik (1966). For the upper phase, the governing equation and boundary conditions are expanded in powers of k as

$$\Phi = \Phi_0 h_0 + k h_1 \Phi_1 + \cdots \quad [8a]$$

$$h = h_0 + k h_1 + \cdots. \quad [8b]$$

For k^0 the no slip boundary conditions are

$$\Phi_0 = \Phi_0' = 0, \quad @y = 1 \text{ (flat wall)}, \quad [9a]$$

$$\Phi_0 = 0, \Phi_0' + U_b' = 0, \quad @y = 0 \text{ (wavy wall by using domain perturbation)}, \quad [9b]$$

and the governing equation is

$$\Phi_0^{iv} = 0. \tag{10}$$

For k^1 order, the boundary conditions are

$$\Phi_1 = \Phi_1' = 0, \quad @y = 1 \text{ (flat wall)}, \tag{11}$$

$$\Phi_1 = 0, \Phi_1' + U_b' = 0, \quad @y = 0 \text{ (wavy wall)}, \tag{12}$$

and the governing equation is

$$R^{-1}\Phi_1^{iv} = i(U_b\Phi_0'' - U_0''\Phi_0). \tag{13}$$

These are easily solved to obtain

$$\Phi_0(y) = -6U_r(y - 2y^2 + y^3) \tag{14}$$

and

$$\Phi_1(y) = \frac{3i}{35} U_r y(y-1)^2(70i + RU_r y - RU_r y^2 - 3RU_r y^3 + 2RU_r y^4). \tag{15}$$

The term U_r is the ratio of the average gas to the average liquid velocity.

To solve the eigenvalue problem in the liquid for the imposed stress model, the expansion for the liquid disturbance stream function is

$$\phi(y) = \phi_0(y) + k\phi_1(y) + \cdots. \tag{16}$$

The boundary conditions at k^0 order are the no slip conditions

$$\phi_0 = \phi_0' = 0 \ @y = -1/d \text{ (flat wall)}, \tag{17}$$

and shear stress and pressure match,

$$\phi_0'' - \frac{\phi_0 u_b''(0)}{u_b(0) - c_0} = -\frac{\mu\phi_0}{u_b(0) - c_0}(\Phi_0'' + U_b''(0)), \quad @y = 0 \text{ (shear stress match)}, \tag{18a}$$

$$\phi_0''' = -\frac{\mu\phi_0}{u_b(0) - c_0}\Phi_0''' \quad @y = 0 \text{ (pressure match)}. \tag{18b}$$

The governing equation is

$$\phi_0^{iv} = 0. \tag{19}$$

Note that the right sides of [18a] and [18b] differ from the expansions of [1] given in Blennerhassett (1980). Also note that the interfacial velocities are not continuous with this model. At k^1 order we have

$$\phi_1 = \phi_1' = 0 \ @y = -1/d \text{ (flat wall)}, \tag{20}$$

$$\phi_1'' - \frac{u_b''(0)}{u_b(0) - c_0}\left(\phi_1 + \frac{\phi_0 c_1}{u_b(0) - c_0}\right) = -\frac{\mu}{u_b(0) - c_0}(\Phi_1'' + U_b''(0))\left(\phi_1 + \frac{\phi_0 c_1}{u_b(0) - c_0}\right), \quad @y = 0 \tag{21}$$

$$\frac{\phi_1'''}{\nu R} - i(\phi_0'(u_b(0) - c_0) - \phi_0 u_b'(0)) + \frac{i(1-\rho)\phi_0}{u_b(0) - c_0}\frac{F}{R^2}$$

$$= \frac{-\rho}{R(u_b(0) - c_0)}\left(\phi_1 + \frac{\phi_0 c_1}{u_b(0) - c_0}\right)\Phi_1''' - \frac{i\rho\phi_0}{(u_b(0) - c_0)}(-\Phi_0' U_b(0) + \Phi_0 U_b'(0)) \quad @y = 0 \tag{22}$$

with the governing equation being:

$$i(u_b - c_0)\phi_0'' - iu_b''\phi_0 = (\nu R)^{-1}\phi_1^{iv}. \tag{23}$$

These equations can be solved analytically to obtain c_0, which is

$$c_0 = \frac{12\mu U_r}{d^3} + \frac{6\mu U_r}{d^2} - \frac{3\mu U_r}{d} + \frac{3\bar{u}_1^+}{U_m^+}. \quad [24]$$

The expression for c_1 was obtained using a computer algebra program and is quite long and thus is not printed here.

A second procedure that is used is to model the gas phase velocity profile with a polynomial as was done by Pai (1953) and Brodkey (1963). Kadambi (1983) used polynomial profiles to predict the base state for a two-layer flow where both phases are turbulent. Because of his method of non-dimensionalization, it is difficult to obtain the information necessary to evaluate his expressions numerically so we have used a slightly different procedure for determining the base state profiles. The liquid is assumed to be laminar and will have a parabolic profile. The gas phase will be turbulent so following Brodkey (1963), an expression for the eddy viscosity, ϵ/ν_2 is

$$\frac{\epsilon(y)}{\nu_2} = \frac{-s}{a_1 + na_2(y - \frac{1}{2})^{2n-2}} \quad [25]$$

where s is the ratio of the shear stress for turbulent flow to the value for laminar flow with the same maximum velocity, a_1 and a_2 are constants that were obtained from the boundary conditions and n is the empirical value of the polynomial order. If [25] is used, the principal assumption in applying the polynomial profile to a two-layer flow is that the eddy viscosity is symmetric. This differs from Kadambi (1983) who assumed that the velocity profiles were symmetric, but that a virtual interface existed. The eddy viscosity is used in the governing equation for the gas phase to give

$$0 = -\frac{\partial P}{\partial x} + \frac{\partial}{\partial y}\left((\epsilon(y) + \nu_2)\frac{\partial U_2}{\partial y}\right), \quad [26]$$

which is then solved with the boundary conditions of no slip or flow through the solid walls and velocity and shear stress match at the gas–liquid interface to give the liquid profile

$$u_L(y) = u_{L0} + u_{L1}y + u_{L2}y^2, \quad [27a]$$

where

$$u_{L0} = (-4(1+d)\mu s(s-2n))/\Delta \quad [27b]$$

$$u_{L1} = (-4\mu s(-2d^2n + d^2s - \mu s + 2\mu ns))/\Delta \quad [27c]$$

$$u_{L2} = -4\mu s \quad [27d]$$

and the gas profile

$$U_G(y) = U_{G0} + U_{G1}y + U_{G2}y^2 + U_{G2n}y^{(2n)} + U_{G2n1}y^{(2n-1)} \quad [28a]$$

where

$$U_{G0} = -(-2d^2n + d^2s + d\mu s - 4\mu ns - 6d\mu ns + 2\mu s^2 + 2d\mu s^2)/\Delta, \quad [28b]$$

$$U_{G1} = (-2(1+d)\mu(-1+2n)(n-s)s)/((n-1)\Delta), \quad [28c]$$

$$U_{G2} = (-n+s)/(n-1), \quad [28d]$$

$$U_{G2n} = (1-s)/(n-1), \quad [28e]$$

$$U_{G2n1} = (-2(1+d)\mu n(-1+s)s)/((n-1)\Delta), \quad [28f]$$

and

$$\Delta = d(2dn - ds - \mu s + 2\mu ns). \quad [28g]$$

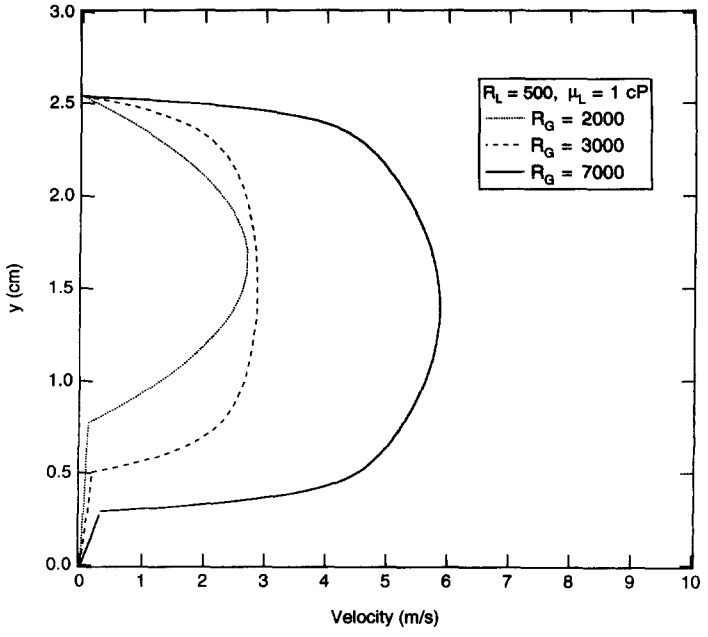

Figure 2. Two-phase velocity profiles as predicted using the polynomial profile for the gas phase. The gas flow is laminar at $R_G = 2000$.

Figure 2 shows the profiles as a function of gas Reynolds number, $R_G = \bar{U}_2^+ D_2^+ / \nu_G$ for fixed R_L. The values of s and n are given by Brodkey (1963) as,

$$n = -0.617 + (8.211 \times 10^{-3}) R_G^{0.786}, \quad [29]$$

$$s = 1 \; R_G < 2040, \quad [30a]$$

$$s = 2.417 \times 10^{-12} R_G^{3.51}, \; 2040 \leqslant R_G \leqslant 2800, \text{ and} \quad [30b]$$

$$s = 0.585 + (3.172 \times 10^{-3}) R_G^{0.833}, \; R_G > 2800. \quad [30c]$$

These predict velocity profiles reasonably well for single phase flow. How well they work for a gas–liquid flow is open to question, but they are included here to show the effect of a simulated turbulent velocity profile. Because the gas–liquid interface will experience lower stress than a solid wall, it is likely that the polynomial profile will predict a more severe effect of turbulence (while ignoring possible dynamic effects) than actually occurs, so it is useful as a limiting case.

3. RESULTS

The first question that arises is how to compare the results of different models. The results of this paper will affirm the importance of the two-layer base state on stability behavior. Interfacial shear is the driving force for instability and liquid depth tells how the fluid will respond. Thus for fixed fluid properties and channel depth a plot of interfacial friction velocity, v_i^* (where v_i^* is the liquid friction velocity defined as $\sqrt{\nu_l \partial u_b^+(0)/\partial y^+}$), versus liquid depth, D_l^+, shows how the models behave based on the mechanism of stability. The effect on stability of different base states for different models is largely removed. Figure 3 gives stability boundaries for the two-layer laminar longwave analysis, our polynomial gas–laminar liquid long wave analysis, Kelvin–Helmholtz ([7], using laminar stresses to get v_i^*) (Lin & Hanratty 1986; Crowley *et al.* 1993) and a two-layer laminar analysis that is showing the short wave boundary. Several observations are in order. Comparing first the two laminar–laminar results, short waves are unstable at lower interfacial friction than long waves. This is consistent with experimental observations (e.g. Hanratty & Hershman 1960; Cohen & Hanratty 1965). However, it is interesting that for sufficiently large liquid depth, the lines cross and long waves are unstable first. A second observation is the lack

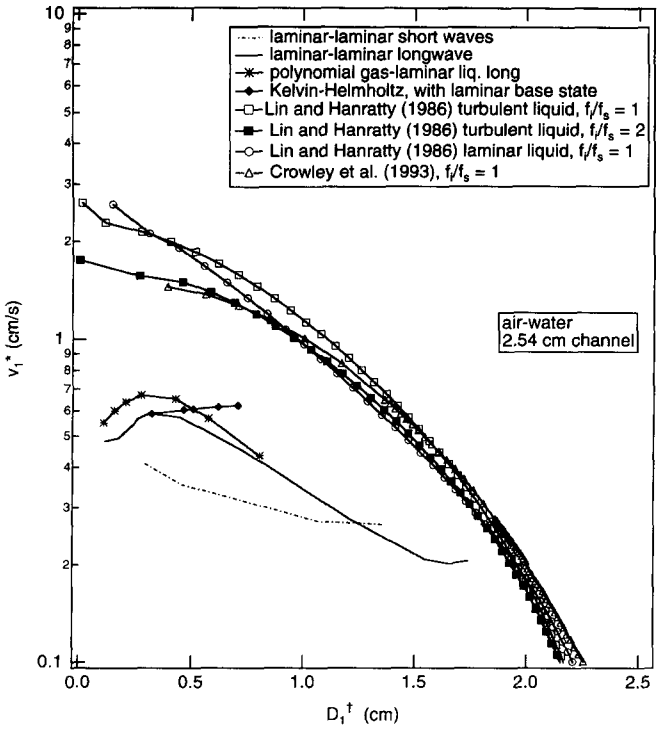

Figure 3. Linear stability boundaries for different models on friction velocity–liquid height coordinates. Stable regions are below the curves, unstable regions are above and to the right of the curves. This plot is intended to remove the effect of different base states and specific value input constants.

of agreement between Kelvin–Helmholtz and laminar short waves. The reason is that Jeffrey's mechanism (Hanratty 1983), which through the pressure fluctuation in phase with the wave slope leads to reinforcement of the orbital motions of traveling waves, is completely absent in the Kelvin–Helmholtz analysis. Note that the interfacial friction velocity drops at low film thickness because there is an impending transition to Craik's (1966) slow waves that exist on thin layers.

Next the macroscopic models will be examined. On these coordinates, all the macroscopic models predict about the same results. The differences that they exhibit in other coordinates (e.g. see figure 4), are due largely to changes in the base state. Even if f_i/f_s (the ratio of the interfacial friction factor to the interfacial friction factor for a smooth interface) is increased to 2—a value which has been shown by Lin & Hanratty (1986) to match slug transition data, there is little change in the prediction in these coordinates. The most important comparison from the standpoint of regime transition is the macroscopic models with the differential longwave analyses. It is seen that there is a disagreement by a factor of 2–3 in the friction velocity required to cause instability at small height; this difference decreases somewhat with increasing height. Consequently it can take substantially more interfacial stress to cause instability for one-dimensional equations as compared to the full differential equations. The polynomial profile gas profile that simulates the effect of turbulence is very close to the laminar result when plotted in this figure. Of course the gas flow rate required to cause the stress is much lower if the flow is turbulent compared to laminar so that the polynomial model also changes stability primarily through changes in the base state.

To show how the comparison of different models changes with coordinate axes, the long wave models and Lin & Hanratty (1986) are plotted in figure 4 on a Mandhane *et al.* (1974) plot as liquid superficial velocity, U_{SL} versus gas superficial velocity, U_{SG}. This provides a comparison in terms of flow rates of the two phases. In this figure the friction factor ratio, f_i/f_s causes a large change in the prediction. Lin & Hanratty's (1986) laminar liquid model predicts instability at lower flow rates than the turbulent liquid model. The macroscopic turbulent liquid model still differs substantially from the differential laminar model, but the macroscopic laminar model is close to the differential laminar model. However, this agreement is coincidental because when the liquid

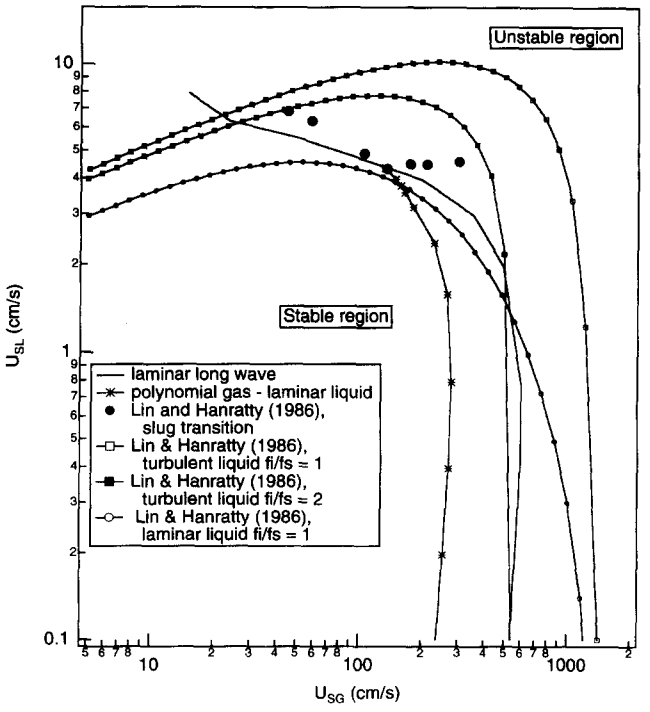

Figure 4. Stability calculations and slug transition data shown in Mandhane coordinates for a 2.54 cm channel. Waves are unstable above and to the right of the curves.

viscosity is increased to 20 cP, the differential and macroscopic models are again very different. At low U_{SG}, the macroscopic curve is below the differential curve; above $U_{SG} = 50$ cm/s, the differential model is below indicating instability at lower U_{SL}. The polynomial gas model shows the expected effect of turbulence, which is that the flow is unstable at gas flow rates lower than laminar. Note the point at which the gas Reynolds number reaches about 2040 is where the polynomial and laminar models intersect. Also shown on this plot are slug transition data of Lin & Hanratty (1986). It is seen that these occur in the range of unstable waves as predicted by our differential models. It is gratifying that the slugs occur in the unstable region. However, it should be emphasized that linear theory predicts only that long wave disturbances are unstable and will grow, it cannot predict if large amplitude disturbances will be observed in a finite length flow system.

Figure 5 shows laminar long wave stability on a liquid versus gas Froude number plot with $a(\rho_G/\rho_L)^{1/2}$ correction for the gas. These axes are essentially the same as those recently introduced by Crowley *et al.* (1993). The exponent on the density correction was also suggested by Andritsos *et al.* (1989). For the two-layer laminar calculations the channel height, gas pressure and liquid viscosity are varied. These calculations produce two distinct regions. One is a nearly constant abscissa $\cong 0.3$, which corresponds to liquid depths that are much less than 1/2 of the channel height. In this region, instability is caused by a sufficient degree of gas shear. Note that even for $\mu_L = 623$ cP, this value does not move much. Evidently, the density-corrected Froude number captures stability behavior in this region as the different conditions collapse very well. The other region is ordinate $\cong 0.1$, about which there is considerable scatter. This is the thick film region where the liquid depth may approach the entire channel height. Results from the polynomial profile are not shown on this plot but they would have the same horizontal asymptote, because the liquid is laminar. The vertical asymptote would move to about 0.1 with little change in the scatter of the lines. The comparison of the Crowley *et al.* (1993) calculations with laminar long wave stability is similar to the comparison of figure 4. The models converge or cross for high liquid flows where the gas is laminar. As the gas flow rate is increased, the laminar model shows a significantly lower value of the gas flow at transition.

The disagreement between the differential models and the macroscopic equations is troubling although not surprising given the significant simplification of the governing equations that is involved. Hanratty (1983) and Lin & Hanratty (1986) emphasize the importance of predicting the interfacial perturbation stresses. They decompose the interfacial pressure and shear stress into real and imaginary components. The real components P_{SR} and τ_{SR} are in phase with the wave height; the imaginary components, P_{SI} and τ_{SI} are in phase with the wave slope. In our notation, the dimensional perturbation pressure or shear stress can be retrieved by multiplying these by $a^{\dagger}D_i^{\dagger}/(\rho_i \bar{u}_i^{\dagger 2})$, where $a^{\dagger}$ is the wave amplitude. Figure 6 shows perturbation shear stresses from the laminar–laminar two layer, laminar divided attack, macroscopic momentum equations of Hanratty (1983) and model D^* from Abrams (1984). Note that in the laminar–laminar long wave stability calculation, the first two powers in k are involved. Thus both the magnitude and limiting slope of the stress components should be compared. In the long wave limit it is seen that all the models agree for the perturbation shear stress so it is not likely to be the reason for the disagreement in the calculations. However, the macroscopic model is not close to the two-layer laminar result for either the real or imaginary component of the pressure. The sign of the slope and value of P_{SR} are different. The different values of perturbation pressure can certainly explain part of the disagreement in the stability boundaries, but the differences in the equations will also contribute.

The stresses from Abrams are included to show values for measured turbulent flow over a solid surface. They could be used in wave stability calculations if two basic questions could be answered. First, what is the error in the divided attack for different values of parameters? Second, what happens to the validity of the turbulent flow data as the wavelength becomes comparable or larger than the channel height? Note that the wavy surface data were taken under conditions where the presence of a top wall was thought to be unimportant. The first question is addressed by comparing the stresses for the two-layer laminar flow with the divided attack laminar. Note that the shear stresses are close but there is some quantitative disagreement. The values for P_{SR} and P_{SI} are almost identical until k/d gets to about unity. In the range of 1–8 they differ somewhat and note that P_{SI} exerts a very strong influence on the growth rate.

It is difficult to draw firm conclusions about the validity of the divided attack from the stresses. Thus in figures 7(a) and 7(b), long wave stability boundaries are constructed in R_G versus R_L

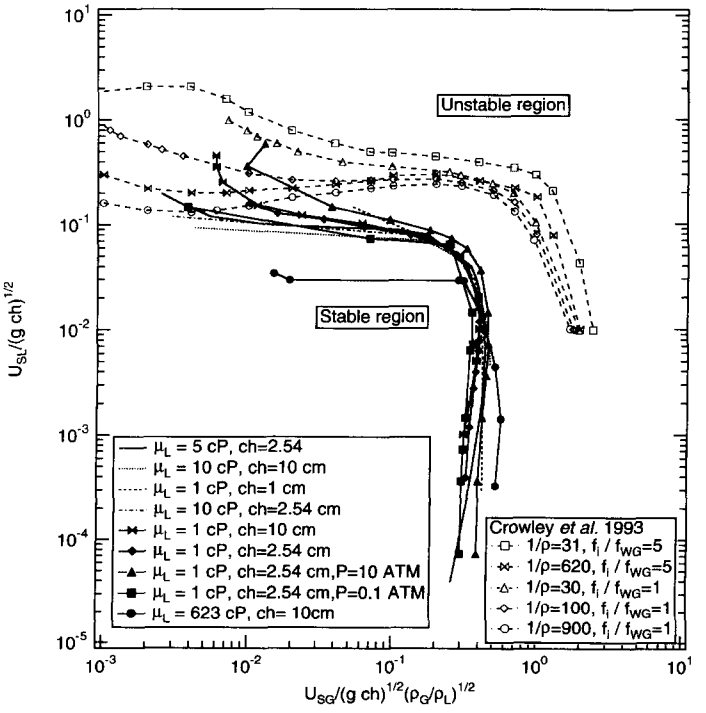

Figure 5. Dimensionless plot of long wave stability. Waves are unstable above and to the right of the curves.

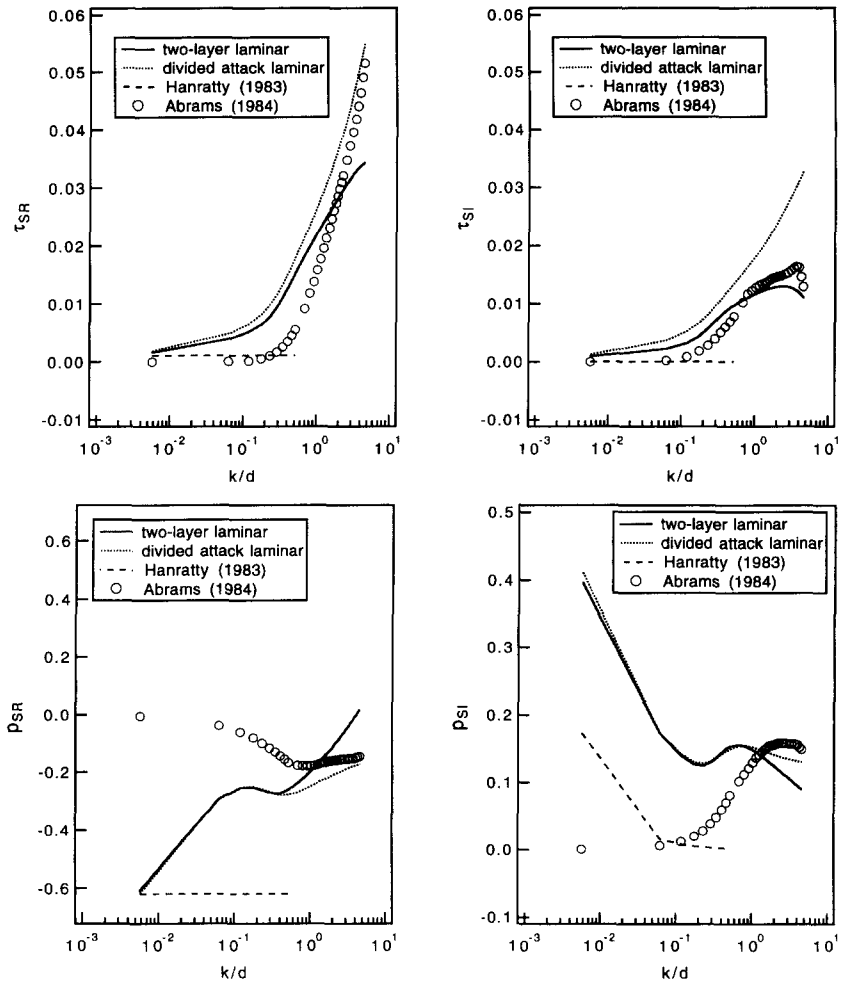

Figure 6. Interfacial stress perturbations from different models, $R_G = 6426$. For the two-layer laminar model, $R_L = 740$, $D_l^+ = 0.57$ cm and the liquid is water.

coordinates for different viscosity and density ratios. Figure 7(a) shows that for the air–water case, the density and viscosity ratios are small enough that the divided attack and two-layer laminar agree. However, as the viscosity ratio is increased towards unity, significant disagreement exists and it becomes larger as R_L is increased. Figure 7(b) shows similar behavior for a changing density ratio. The useful result from this figure is that for gas–liquid flows, the long wave stability can probably be explained using the divided attack which could allow use of either elaborate turbulent models, measured data from solid waves or numerical simulations of gas flow turbulence in the stability calculations.

It is interesting to examine the divided attack over the entire wavenumber range. Figure 8 shows a comparison of the growth curves for a two-layer laminar flow, the divided attack model using the turbulent stress correlations of Abrams and a laminar gas divided attack model (the full wavelength numerical version of [8]–[23] above). The liquid Reynolds number is 740 and laminar values for R_G are 1965, 3516, 4558 and 6426. Note that the actual turbulent R_G for the last three will be smaller than the laminar values. The fluids are air–water and in all cases the laminar base state is used to calculate the height and friction velocity. It is seen that, as expected for the long wave region, the differences in the growth rate between the two-layer laminar and the divided attack laminar are very small. For k/d greater than unity, the divided attack consistently predicts a higher growth rate for the entire range. While the difference is not due entirely to the stresses, P_{SI} is higher for this range for the divided attack. The magnitude of the growth of any particular wavenumber

is not much different for the divided as compared to the full solution and it is not clear if this difference would be detectable in experiments. However, the integral of the growth rate over all frequencies can be quite different and it is possible that this could lead to differences in the energy in the entire wave spectrum. The third set of curves that use Abrams' stresses reveal new information. First there are only minor differences in growth rates for the laminar and turbulent divided attack if k/d is greater than 2. This suggests that turbulence is having only a minor effect on the stability calculation. For k/d below unity significant differences occur. For the three highest R_G values, Abrams' stresses predict stable long waves while the laminar models predict unstable long waves! This is a serious discrepancy. While this could be due to turbulence, these values of k/d are below the wavenumber region where the turbulent data show large differences from his laminar predictions. It is likely that the error is due to the wavelength becoming long compared to the gas height. The values of k/d where the error occurs are well within the $\alpha^+ (= 2\pi v_2/\lambda v_2^*$, where v_2^* is the gas friction velocity defined as $\sqrt{v_2 \partial U_b^+(0)/\partial y^+}$ and λ is wavelength) values of the measurements so this is not the problem.

From the results above, it is expected that laminar–laminar stability calculation can be used to provide insight into turbulent flows if the liquid height and friction velocity are the same. Thus this calculation procedure will be used to examine several questions related to linear wave growth.

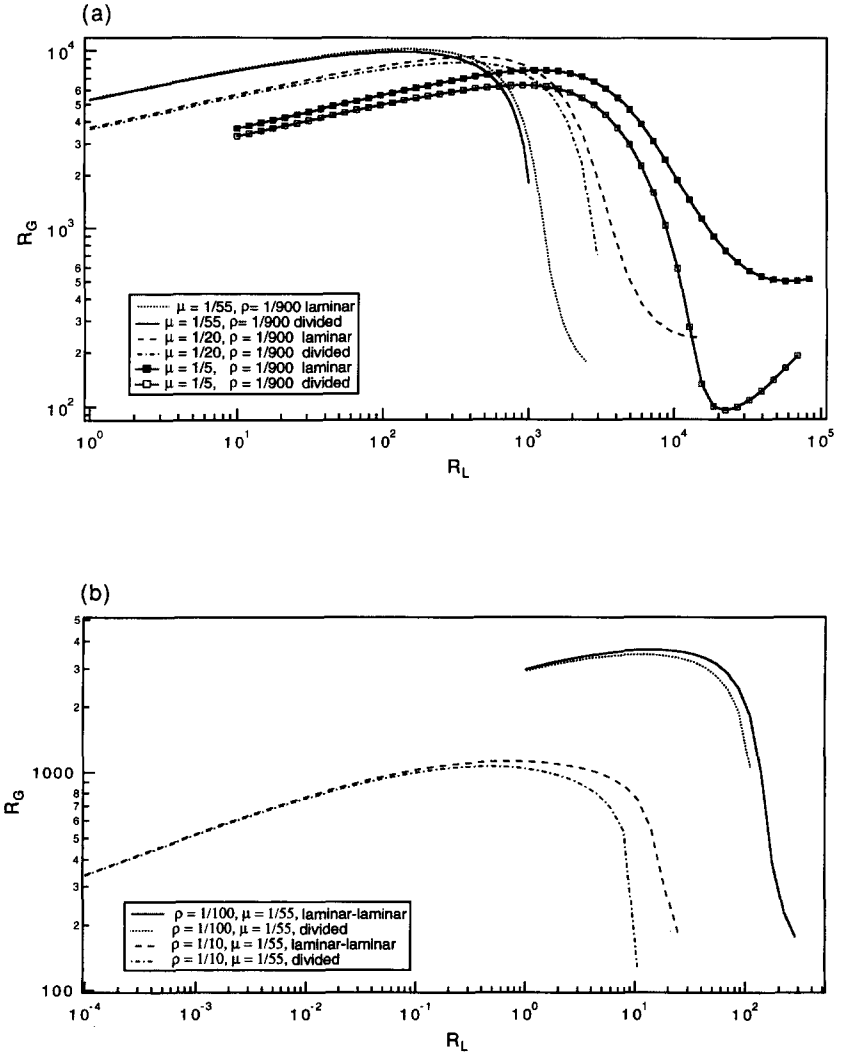

Figure 7. (a) Long wavelength stability boundary for divided attack and two-layer laminar for different viscosity ratios. (b) Long wavelength stability boundary for divided attack and two-layer laminar for different density ratios.

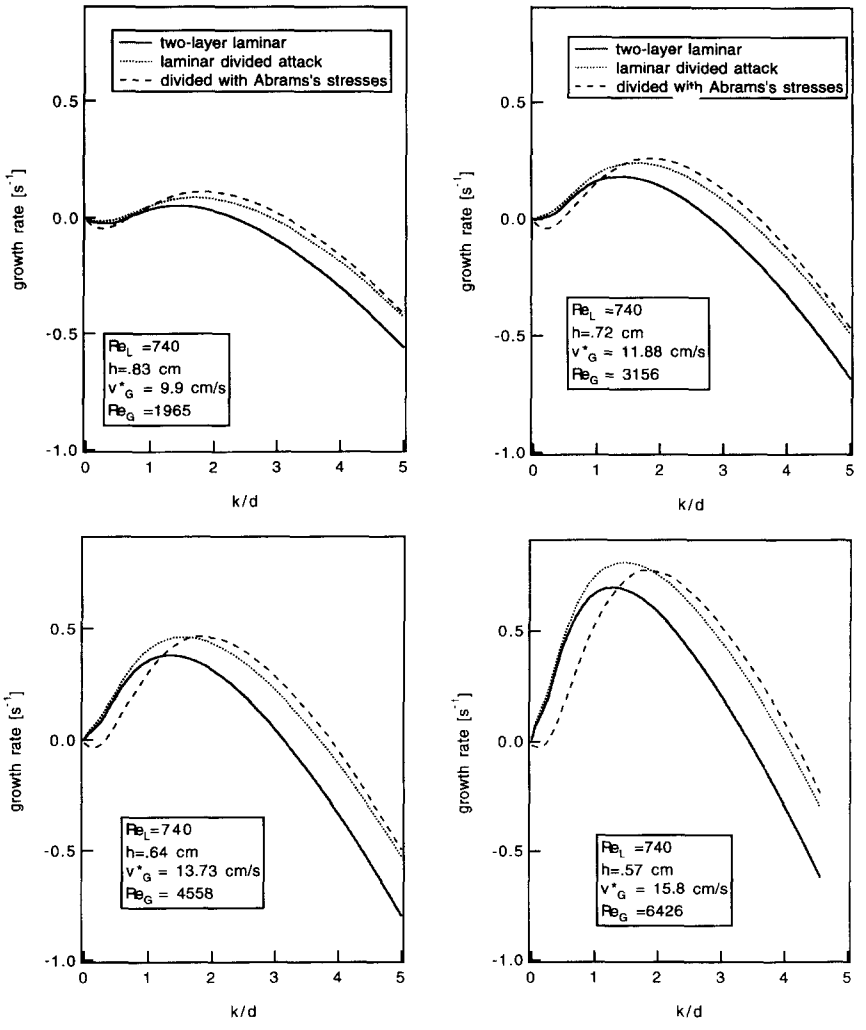

Figure 8. Growth rate curves for the air–water system comparing the two-layer laminar, the divided attack laminar and the divided attack using Abrams' stresses.

The effect of the changing pressure on the moderate wavelength stability is shown in figure 9(a). This figure simulates (and exaggerates) the effect of a compressible gas in a long pipeline where the gas flow rate is constant but pressure changes lead to changes in the liquid height and gas velocity. It is seen that as the pressure decreases, the growth rate increases dramatically because the increased gas velocity causes greater interfacial shear. Figure 9(b) shows that the curves can be partially collapsed by using non-dimensional wavenumber and a growth rate made dimensionless with the friction velocity and liquid depth.

The overall effect of the conservative forces gravity and surface tension can be determined from figure 10 where the speed and growth rate are plotted for $g = 980\,\text{cm/s}^2$ and $g = 0$ while $S = 72$ dyne/cm and then for $g = 980\,\text{cm/s}^2$ and $S = 0$. The wave speed for $g = 980\,\text{cm/s}^2$ is much larger at low wavenumber than for $g = 0$ because gravity is the restoring force that causes the disturbance to travel—as opposed to remaining stationary. The difference in speed explains the growth curve differences. If $g = 0$, growth of long wavelength waves is opposed only by the viscous action of the bottom wall. Slower waves encounter less viscous resistance and therefore have larger growth rates. For $g = 980\,\text{cm/s}^2$, the higher wave velocity and the direct action of gravity as a restoring force lead to a much lower growth rate. As the wavenumber is increased, surface tension becomes the dominant restoring force and the speeds and growth curves approach each other. Surface tension is responsible for increasing the wave speed at increasing wavenumber. The

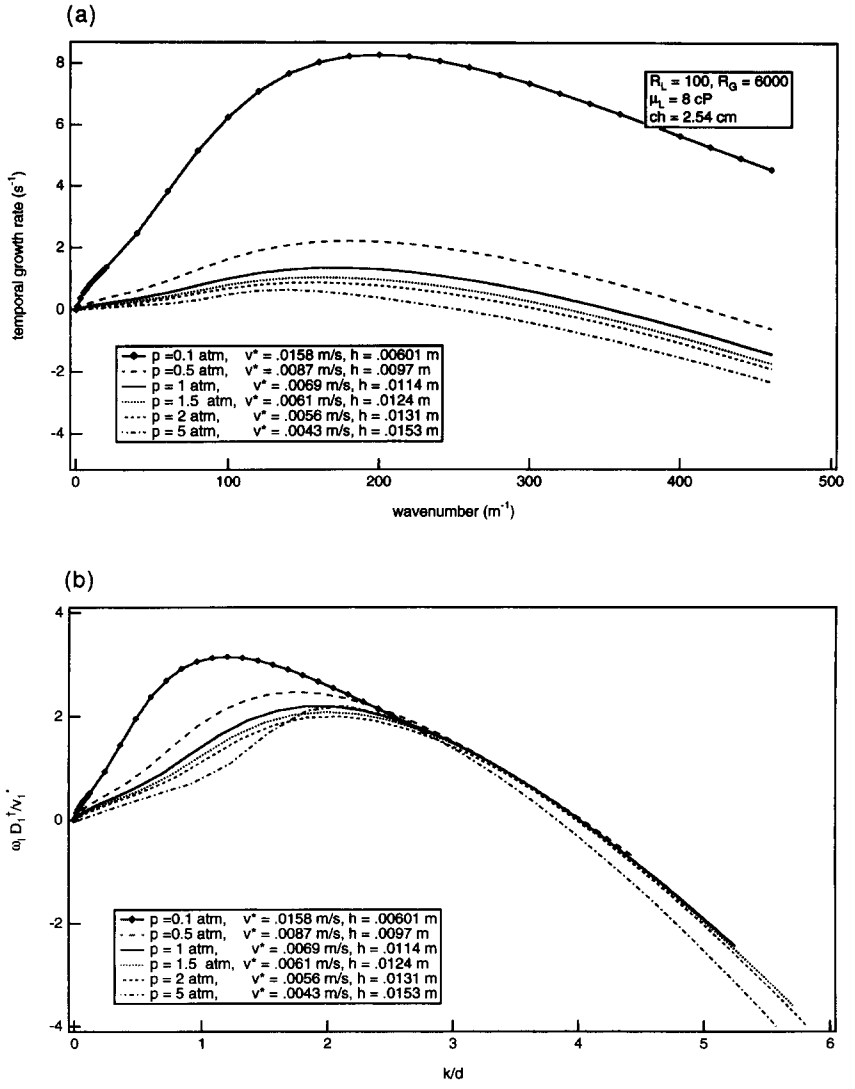

Figure 9. (a) Effect of pressure on growth curve for constant mass flow rate (dimensional). (b) Effect of pressure on growth curve for constant mass flow rate shown in dimensionless variables.

increased speed leads to more dissipation and therefore a lower growth rate than if surface tension were not present. Note that surface tension is not needed to stabilize waves in the range of the peak growth rate. The growth curve for $S = 0$ eventually turns upward, but waves do not become unstable unless the wavelength is less than about 0.018 cm ($k^+ = 35{,}000$/m).

Figure 11 shows linear growth curves for conditions that are not typical. It is important for two reasons. In figure 3, over most of the range, short waves are unstable at less severe conditions than long waves. This is the expected case. Consistent with figure 8, the wavenumber of the peak is about order one. Figure 11 shows an example of conditions where long waves can become unstable before short waves. Second, it is possible that both long and short waves are unstable with an intermediate stable region. The second point is relevant to the question of energy transfer through the wave spectrum. If energy transfer occurs by non-linear interactions, experiments and theory show that it is difficult to excite a stable mode. Thus stable intermediate modes can interfere with the energy transfer from short waves to long waves. This process may be important in the generation of roll waves and other long disturbances because the growth rate in the long wave region is never as large as typical short wave values.

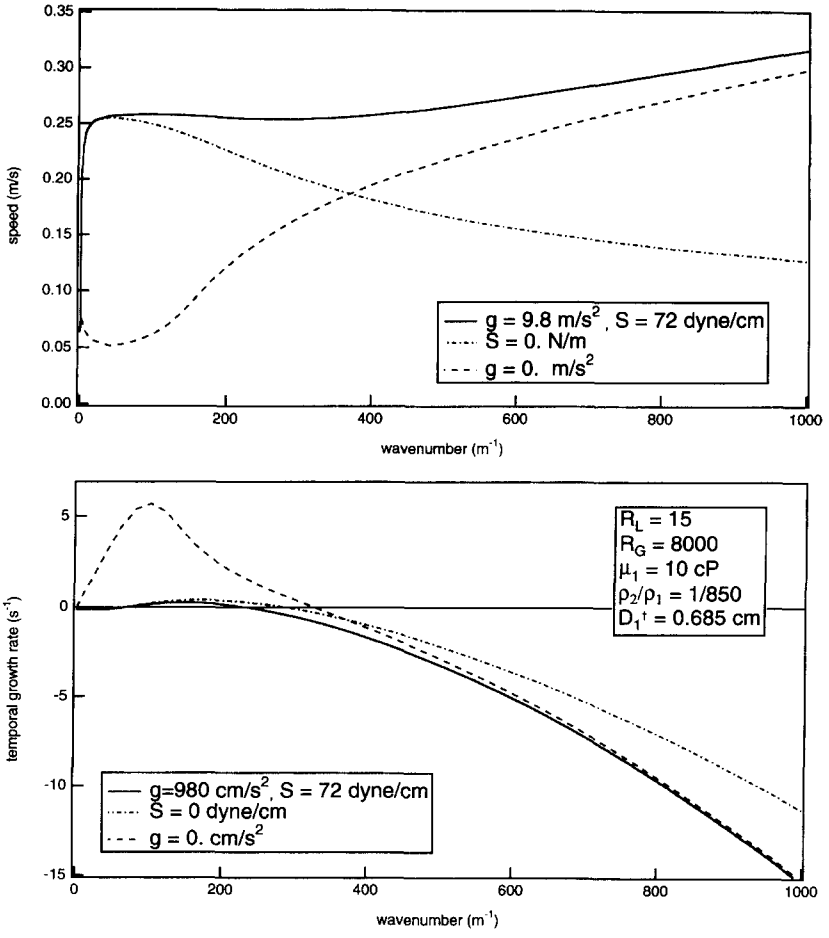

Figure 10. Comparison of speed and growth rate for each gravity versus $g = 0$ and normal surface tension versus no surface tension. The absence of gravity as a restoring force causes a large change in the speed for low wavenumber. The effect of surface tension is less dramatic.

The results above show the importance of the friction velocity and liquid height on stability. Thus it might be expected that some simple relation exists that could be used to correlate the neutral stability curve for short waves even though six parameters govern the process. To test this hypothesis, we have plotted the neutral curve for short waves for several different sets of fluid properties and channel heights. It is seen that getting a simple correlation is unlikely because the v_l^* versus $D_l^\dagger$ plots are not monotonic. Apparently, although the required gas flow rate usually decreases with increasing liquid flow, the reduced gas space leads to a higher interfacial shear. Figure 12 also shows that changing surface tension does not move the neutral curve very much. This is expected if the viscosity ratio is sufficiently different from unity.

Figure 13 shows a correlation of growth rates predicted from calculation for moderate waves plotted as $\omega_l D_l^\dagger / v_l^*$, where ω_l is the dimensional wave growth rate, versus $(R_G - R_{Gcrit})/R_{Gcrit}$. The reduced gas Reynolds number contains R_{Gcrit} which is the value of R_G for the onset of waves. In this plot all the conditions do not lie on the same line. However, the slope is close to unity on this log–log plot, so it is easy to determine changes in growth rates with R_G.

4. DISCUSSION

4.1. *Accuracy of simplified models*

The results in figures 3–5 show clearly that the one-dimensional momentum model, which omits the effects of important velocity derivatives, and Kelvin–Helmholtz, which omits the effects of

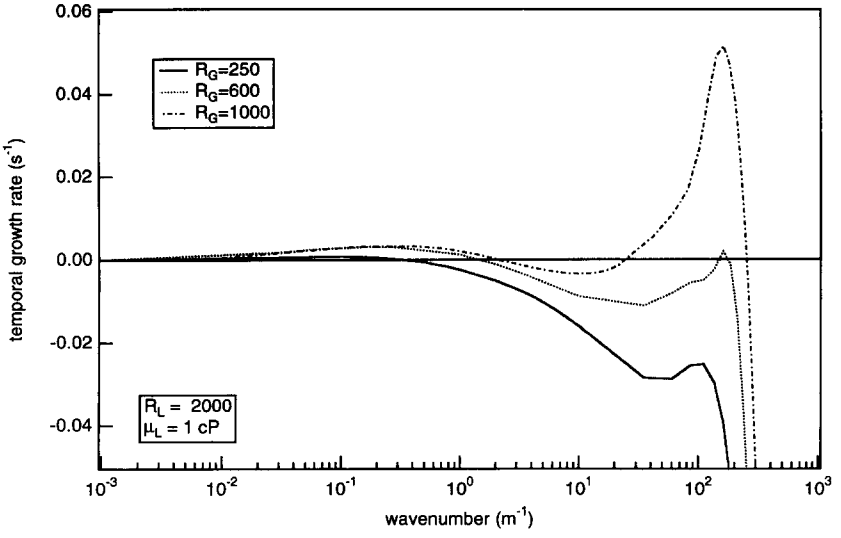

Figure 11. Conditions where long waves are more unstable than short waves.

interfacial shear and liquid inertia, do not accurately predict linear stability of interfacial waves for either long or moderate wavelengths. It is probably possible to correct these in certain regions to match the exact calculations but it is not clear if this would be a worthwhile exercise. It is relatively easy to implement all the procedures that we have used to obtain solutions of the exact equations so it is probably best to base future studies on the complete differential equations. One point is clear, if the simplified models show agreement with, for example, transition to annular flow or slugging, then the observed phenomena are not the direct result of a linear instability, or the agreement is fortuitous because of limited parameter range or length of flow system.

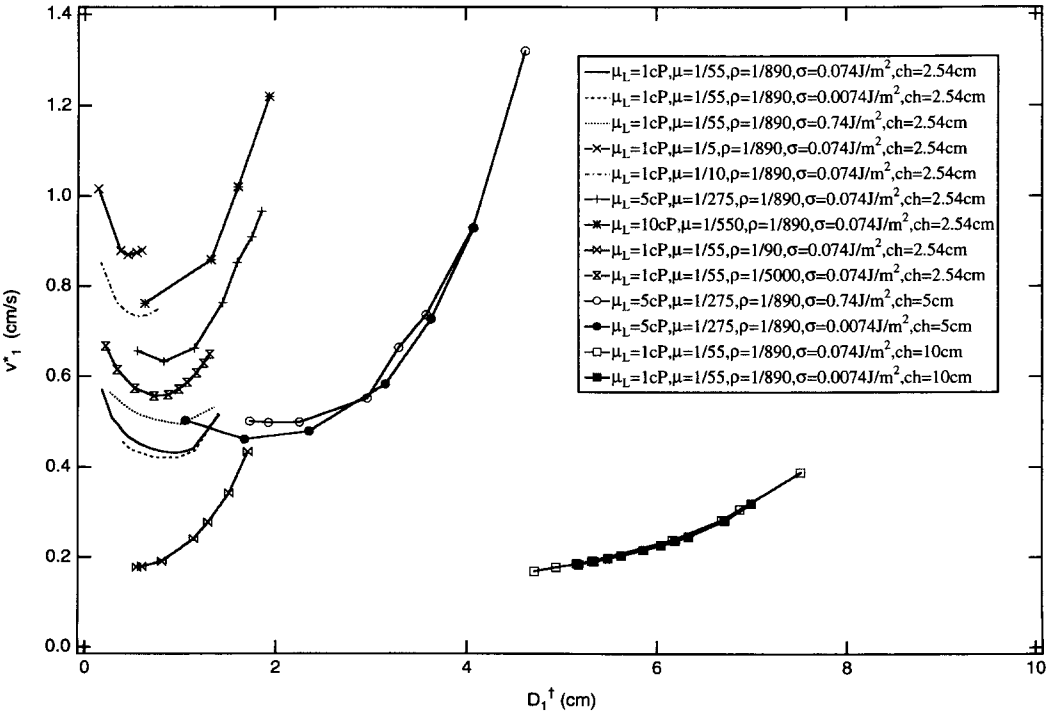

Figure 12. Short wave stability boundary for different fluid properties and channel height on friction velocity—liquid depth coordinates.

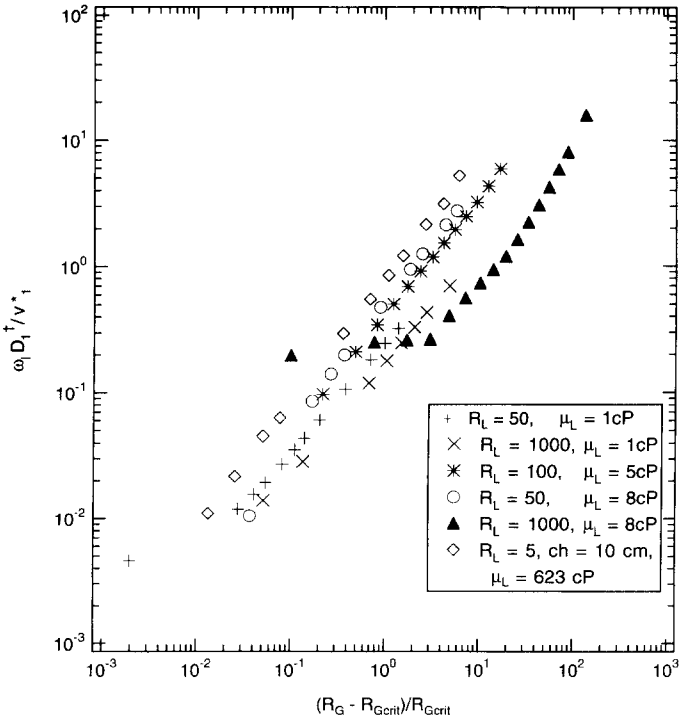

Figure 13. Plot of dimensionless growth rate and reduced gas Reynolds number.

4.2. *Effect of turbulence*

The results presented here demonstrate that the effect of turbulent flow is largely through changes in the base state. For fixed R_G, the friction velocity and pressure drop are higher and the liquid thickness is lower for turbulent flow. If the liquid height and friction velocity are the same as laminar flow, the effect of turbulence is not large. Some effects could be missed because of a lack of a two-phase code that possesses Reynolds stresses, however the similarity of the growth curves in figure 8 argues against this. It is likely that the primary quantitative effect of turbulence is to skew the growth curve to slightly higher wavenumbers.

For design purposes, stability of the long wave region can be predicted from either the two-layer laminar or the polynomial profiles as long as R_G can be adjusted to give the correct interfacial shear. The imposed stress model is recommended only if the viscosity and density ratios or R_L are sufficiently small. For moderate wavelength waves, the divided attack approach is not very accurate and any improvements in the representation of the gas flow by using a turbulence model are not likely to be realized. A better method for dealing with stability of turbulent flow is desirable, but does not seem essential, so that primary effort in the short term should probably concentrate on correctly predicting the base state.

4.3. *Stability of moderate wavelength waves*

If a flow is stable to both long and moderate wavelength disturbances, the regime will remain stratified. Figure 5 is useful for long wave stability but it appears that moderate to short wave stability can be calculated only from the complete equations. It is noted that high wavenumber, high R_L approximations such as Cohen & Hanratty (1965) fail for moderate wavenumbers that are fastest growing. Moderate wavelength waves roughen the surface and increase pressure and interfacial mass transfer rates. Methods that estimate the amplitude of waves may be based on equations for individual modes (e.g. Jurman *et al.* 1992) or equations for predicting the entire spectrum (e.g. Bruno & McCready 1988). Linear growth rate is the most important input parameter for each method and it can be obtained from figure 13.

4.4. *Importance of long wave stability on flow regime transition*

Fan *et al.* (1993) observed period doubling of the primary wave peak for conditions close to slug formation for $U_{SG} < 3$ ms/s. This is caused by a non-linear mechanism where the fundamental wave is traveling close to the speed of the subharmonic. Results from Jurman *et al.* (1992) suggest that while a subharmonic can be generated even if it is linearly stable, it will not grow to large amplitude. Thus, it is likely that the subharmonic is unstable in Fan's experiments. If the conditions for slug generation from Fan *et al.* (1993) are plotted on figure 8, they lie in the range of the ordinate = 0.13–0.3 and abscissa = 0.015–0.7; all of these conditions are unstable to long waves. For most situations, the shape of the growth curve is such that if it is unstable to both long and moderate waves, it is unstable to all intermediate wavenumbers (figure 11 is an exception). Thus for slugs to form by the period doubling and growth mechanism seen by Fan *et al.* (1993), it is likely that the flow must be unstable to both long and moderate waves. It is also likely that anytime a flow is unstable to long wave disturbances, it will not remain stratified. For large liquid flow rates either slugs or bubbles will form when the liquid bridges the pipe diameter. For lower liquid rates roll waves will form and sufficient atomization will probably occur for the regime to be considered annular. Long wavelength waves can be stabilized to some extent by non-linear energy transfer to shorter waves, however, it is not likely that this mechanism could dissipate enough energy to stabilize a growing long wave disturbance unless its growth rate is extremely small.

4.5. *Effect of finite length on experimentally observed transitions*

For conditions near the observed transition to slug flow, the growth rate is (very) roughly linear in k up to close to the peak. Thus when the peak growth rate at $\sim 200\,m^{-1}$ is $5\,s^{-1}$, the growth rate of a 1.0^{-1} wavenumber mode would be only $0.025\,s^{-1}$. For a typical wave velocity of say, 0.6 m/s, by linear growth it would take 110 m for the wave to grow 100 times the original amplitude—a value expected to make the disturbance visible. Non-linear energy transfer from shorter waves will shorten this distance somewhat, but these numbers suggest that Fan *et al.*'s warning about the effect of length on slug transition is well founded. If it is necessary to assure that slugs or roll waves will not form no matter how long the distance is, the flow probably must be stable to all disturbances except possibly for a small band at moderate wavenumbers. Experiments of Jurman *et al.* (1992) show how the fastest moderate wavenumber peak is stabilized by overtone formation. However as mentioned above, no experimental evidence exists to show that a long wavelength wave can be stabilized except by breaking.

4.6. *Design recommendations*

Just as it is necessary to know if a flow is laminar or turbulent, it is essential to know if the interface of a gas–liquid flow is unstable. If the flow rates, fluid properties, liquid height and interfacial shear are known, a numerical calculation for a two-layer laminar flow with the gas height and/or velocity adjusted to match the correct liquid depth and friction velocity should give satisfactory results for either laminar or turbulent gas flows. Liquid turbulence was not examined here but its main effect is also likely to be through the base state. Calculation of a single growth curve in figure 8 takes about 5×10^9 floating point operations. This is only a few minutes on a modern workstation. If a complete calculation is not possible and there is some experimental estimate of the R_G of the onset of waves, it is possible to estimate growth rates from figure 13. Steady waves with slopes less than about 0.4 will have amplitudes that scale roughly as the square root of the growth rate. Fortunately, stability of waves with wavelengths long compared to the channel height can be determined without accurate knowledge of the base state. Figure 5 gives reasonably general stability boundaries. Note that it is not possible for a linear theory to determine if unstable wave modes will lead to slug flow as opposed to annular flow. However, the data and discussion by Lin & Hanratty (1986) show that the liquid depth/channel height ratio plays a significant role in deciding whether annular or slug flow will occur.

5. CONCLUSIONS

Linear stability of channel flow is best predicted using the exact differential formulation and a solution procedure that is valid for all wavenumbers because the peak growth rate usually occurs

at dimensionless wavenumber of order unity. Neither the Kelvin–Helmholtz model nor the integral momentum equation approach correctly predicts the onset of disturbances in most cases. The discrepancies in the models are due to more than differences in the calculation of interfacial perturbation stress components and differences in the base states. The effect of gas phase turbulence is modeled with both a polynomial velocity profile and a separated phase approach that employs measured stress correlations for boundary conditions. In both cases the primary effect of turbulence is to cause a higher interfacial stress and larger pressure drop than laminar flow. There is no obvious first order effect on stability or growth rates caused by turbulence *per se* based on the models used in this study; a stability procedure that accurately incorporates Reynolds stresses is needed to verify this statement. It is found that long wave stability can be correlated well using density-corrected gas and liquid Froude numbers. Furthermore, the peak growth rate for moderate wavelength waves increases as a scaled gas Reynolds number to the first power. Under conditions where unstable moderate wavelength waves appear within a couple of meters, it can take 20–50 times this length for slowly growing long wavelength waves, which can destroy regime stability, to appear.

Acknowledgements—This work was supported by the Department of Energy under grant DE-FG02-ER 13913 and NASA Microgravity Science and Applications Division under grant number NAG3-1398.

REFERENCES

Abrams, J. 1984 Turbulent flow over small amplitude solid waves. Ph.D. thesis, University of Illinois, Urbans, IL.

Andritsos, N., Williams, L. & Hanratty, T. J. 1989 Effect of viscosity on the stratified-slug transition in horizontal pipe flow. *Int. J. Multiphase Flow* **15,** 877–892.

Barnea, D. 1991 On the effect of viscosity on stability of stratified gas–liquid flow—application to flow pattern transition at various pipe inclinations. *Chem. Engng Sci.* **46,** 2123–2131.

Blennerhassett, P. J. 1980 On the generation of waves by wind. *Proc. R. Soc. Lond. A* **298,** 451–494.

Brauner, N. & Maron, D. M. 1991 Analysis of stratified/nonstratified transitional boundaries in horizontal gas–liquid flows. *Chem. Engng Sci.* **46,** 1849–1859.

Brodkey, R. S. 1963 Limitations on a generalized velocity distribution. *AIChE Jl* **9,** 448–451.

Bruno, K. & McCready, M. J. 1989 Study of the processes which control the interfacial wave spectrum in separated gas–liquid flows. *Int. J. Multiphase Flow* **15,** 531–552.

Cohen, L. S. & Hanratty, T. J. 1965 Generation of waves in the concurrent flow of air and a liquid. *AIChE Jl* **11,** 138–144.

Craik, A. D. D. 1966 Wind generated waves in thin liquid films. *J. Fluid Mech.* **26,** 369–392.

Crowley, C. J., Wallis G. B. & Barry, J. J. 1992 Validation of a one-dimensional wave model for the stratified to slug flow regime transition, with consequences for wave growth and slug frequency. *Int. J. Multiphase Flow* **18,** 249–271.

Crowley, C. J., Wallis, G. B. & Barry J. J. 1993 Dimensionless form of a one-dimensional wave model for the stratified flow regime transition. *Int. J. Multiphase Flow* **19,** 369–376.

Drazin, P. G. & Reid, W. H. 1981 *Hydrodynamic Stability*. Cambridge University Press, New York.

Fan, Z., Lusseyran, F. & Hanratty, T. J. 1993 Initiation of slugs in horizontal gas–liquid flows. *AIChE Jl* **39,** 1741–1753.

Gardner, D. R., Trogdon, S. A. & Douglass, R. W. 1989 A modified tau spectral method that eliminates spurious eigenvalues. *J. Comp. Phys.* **80,** 137.

van Gastel, K., Janssen, P. A. E. M. & Komen, G. J. 1985 On phase velocity and growth rate of wind-induced gravity–capillary waves. *J. Fluid Mech.* **161,** 199–216.

Hanratty, T. J. 1983 Interfacial instabilities caused by air flow. In *Waves on Fluid Interfaces* (Edited by Meyer, R. E.). Academic Press, New York.

Hanratty, T. J. & Hershman, A. 1960 Initiation of roll waves. *AIChE Jl* **7,** 488–497.

Hanratty, T. J. & McCready, M. J. 1995 Phenomenological understanding of separated gas–liquid flows. *Multiphase Sci. Technol.* In press.

Hinch, E. J. 1984 A note on the mechanism of the instability at the interface between two shearing fluids. *J. Fluid Mech.* **144,** 463–465.

Hooper, A. P. 1985 Long wave instability at the interface between two viscous fluids: thin layer effects. *Phys. Fluids* **28,** 1613–1619.

Hooper, A. P. & Boyd, W. G. C. 1983 Shear flow instability at the interface between two viscous fluids. *J. Fluid Mech.* **128,** 507–528.

Hooper, A. P. & Boyd, W. G. C. 1987 Shear flow instability due to a wall and a viscosity discontinuity at the interface. *J. Fluid Mech.* **179,** 201–225.

Jurman, L. A., Deutsch, S. E. & McCready, M. J. 1992 Interfacial mode interactions in horizontal gas–liquid flows. *J. Fluid Mech.* **238,** 187–219.

Kadambi, V. 1983 Void fraction and pressure drop in two-phase stratified flow. *Can. J. Chem. Engrs* **59,** 584–589.

Kawai, S. 1979 Generation of initial wavelets by instability of a coupled shear flow and their evolution to wind waves. *J. Fluid Mech.* **93,** 661–703.

Kordyban, E. S. & Ranov, T. 1970 Mechanism of slug formation in horizontal two-phase flow. *J. Basic Engng* **92,** 857–864.

Lin, P. Y. & Hanratty, T. J. 1986 Prediction of the initiation of slugs with linear stability theory. *Int. J. Multiphase Flow* **12,** 79–98.

Mandhane, J. M., Gregory, G. A. & Aziz, K. 1974 A flow pattern map for gas–liquid flow in horizontal pipes. *Int. J. Multiphase Flow* **1,** 537–553.

Orszag, S. A. 1971 Accurate solution of the Orr–Sommerfeld stability equation. *J. Fluid Mech.* **50,** 689–703.

Pai, S. I. 1953 On turbulent flow between parallel plates. *J. Appl. Mech.* **20,** 109–114.

Renardy, Y. 1985 Instability at the interface between two shearing fluids in a channel. *Phys. Fluids* **28,** 3441–3443.

Sangalli, M., Prokopiou, Th., McCready, M. J. & Chang, H.-C. 1992 Observed transitions in two-phase stratified gas–liquid flow. *Chem. Engng Sci.* **47,** 3289–3296.

Su, Y. Y. & Khomami, B. 1992 Numerical solution of eigenvalue problems using spectral techniques. *J. Comput. Phys.* **100,** 297–305.

Taitel, Y. & Dukler, A. E. 1976 A model for predicting flow regime transitions in horizontal and near horizontal gas–liquid flow. *AIChE Jl* **22,** 47.

Thorsness, C. B., Morrisroe, P. E. & Hanratty, T. J. 1978 A comparison of linear theory with measurements of the variation of shear stress along a solid wave. *Chem. Engng Sci.* **33,** 579.

Valenzuela, G. R. 1976 The growth of capillary–gravity waves in the coupled shear flow. *J. Fluid Mech.* **76,** 229–250.

Yiantsios, S. G. & Higgins, B. G. 1988 Linear stability of plane Poiseuille flow of two superposed fluids. *Phys. Fluids* **31,** 3225–3238.

Yih, C. S. 1967 Instability due to viscosity stratification. *J. Fluid Mech.* **27,** 337–352.